Diffusion in $Co_{90}Fe_{10}$/Ru multilayers

Erik B. Svedberg[a] and Kent J. Howard
Seagate Technology, Pittsburgh, Pennsylvania 15222-4215

Martin C. Bønsager and Bharat B. Pant
Seagate Technology, Bloomington, Minnesota 55435-5489

Anup G. Roy and David E. Laughlin
Electrical and Computer Engineering Department, Carnegie Mellon University, Pittsburgh, Pennsylvania 15213-3890

(Received 13 February 2003; accepted 30 April 2003)

Signal degradation in spin-valve structures is today a concern for long-term stability of data storage devices. One of the possible degradation mechanisms of spin-valve structures in disk drive applications could be thermally activated diffusion between constituent layers. In order to predict and control performance degradation, the interdiffusion coefficients for all bilayers in the spin-valve structure will have to be determined. Here we report results from a $Co_{90}Fe_{10}$/Ru interface, common in many spin-valve structures. The diffusion in (0002) oriented polycrystalline $Co_{90}Fe_{10}$/Ru multilayers has been measured and quantified by x-ray reflectivity in the temperature range of 450–540 °C. The bulk diffusion in this case is described by an activation energy of $E_a = 4.95$ eV and a prefactor of $D_0 = 6.43 \times 10^{-9}$ m^2/s. No grain boundary diffusion was detected in the large-grain structure dominated by high symmetry grain boundaries at the temperature interval in this study. For a spin-valve structure that contains $Co_{90}Fe_{10}$/Ru interfaces it is clear that with the absence of grain boundary diffusion and a very high activation energy to bulk diffusion degradation will first take place at another interface, or by another phenomenon. © *2003 American Institute of Physics.*
[DOI: 10.1063/1.1586478]

I. INTRODUCTION

For low diffusivity (less than 10^{-23} m^2/s) in thin films, Rutherford backscattering, Auger electron spectroscopy, and secondary-ion-mass spectrometry have insufficient sensitivity.[1] Currently, one of the most sensitive techniques is x-ray diffraction of multilayer structures[2,3] where the decay of satellite-peak intensity is related to interdiffusion of neighboring layers. The theory of interdiffusion in artificial compositionally modulated materials is well developed, and in its simplest form, the equations are linearized by treating several parameters as composition independent.[4]

A multilayer structure can be viewed as periodic modulation of the electron density $c(x)$, and can be described by a Fourier series as[5]

$$c(x) = \sum_{m=-\infty}^{+\infty} A_m \sin\left(m \frac{2\pi}{\Lambda} x \right). \tag{1}$$

In Eq. (1), A_m is the amplitude of the mth order Fourier component, Λ is the modulation length, and x is the growth direction. The intensity of the multilayer x-ray satellite peaks I_m is proportional to the square of the Fourier coefficients: $I_m \propto A_m^2$; see, for example, Ref. 6. Thus, diffusion, which leads to a decrease in modulation amplitude, can be viewed as a decrease in the intensity of x-ray reflectivity peaks. The decrease of satellite intensity is used to calculate the diffusivity in the continuum approach via the following linearized diffusion equation:[4]

$$\frac{d}{dt}(\ln I_m) = -2D\left(\frac{2\pi m}{\Lambda} \right)^2, \tag{2}$$

where D is the effective interdiffusion coefficient. This is a standard method for studying interdiffusion in multilayers and superlattices, and is valid except when the repeated layer thickness Λ is of the same order as the interatomic spacing.[4] From the temperature dependence of the diffusivity, activation energy E_a can be extracted assuming Arrhenius behavior,

$$D = D_0 \exp\left(-\frac{E_a}{kT} \right) \Leftrightarrow \ln D = \ln D_0 - \frac{E_a}{kT}. \tag{3}$$

Equation (3) describes the temperature dependence of the diffusivity where k is the Boltzmann constant and T is the absolute temperature. Thus, by plotting the logarithm of D as a function of $1/T$ the activation energy is given by the slope of the graph. For a more detailed description of the linearized diffusion equation, the reader is referred to Refs. 4 and 7.

II. EXPERIMENT

Multilayers of $Co_{90}Fe_{10}$/Ru were deposited on 3 in. Si wafers with a 100 nm SiO_2 layer by magnetron sputtering in 4 – 5 mTorr Ar gas. The $Co_{90}Fe_{10}$ layer thickness was ~2 nm and the Ru thickness ~1 nm. The 3 nm bilayer was repeated 15 times and capped with an 8 nm TaN cap. The seed layer was 5 nm $(Ni_{80}Fe_{20})_{60}Cr_{40}$. The multilayer structures were subsequently annealed in a rapid thermal annealer (RTA) in which Ar gas was used to continuously purge the quartz chamber. The O_2 levels were monitored during an-

[a]Electronic mail: e_svedberg@yahoo.com

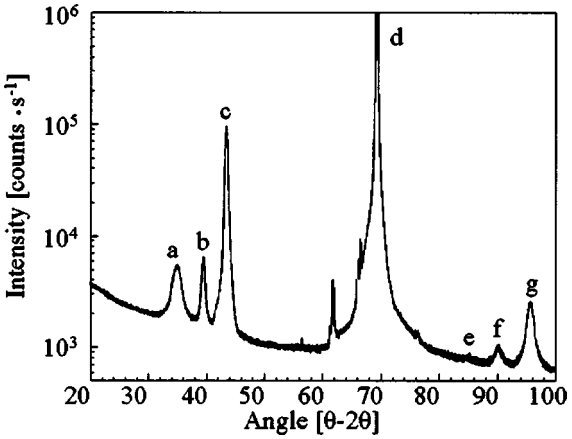

FIG. 1. High angle x-ray diffraction spectra of the as-deposited sample. Peak (a) is the fcc TaN (111) peak from the cap layer while (b) is the primitive cubic NiFeCr seed (200) peak and (c) the hcp (0002) CoFe peak. Peak (d) has a low angle side "tail" from the hcp (0002) Ru peak with slightly larger *c* spacing. At $2\theta = 69.1°$ the Si (400) peak can be seen. Peak (e) is the higher order (400) NiFeCr peak while peak (f) is a separate (0004) Ru peak and peak (g) the (0004) CoFe peak.

nealing and kept below 2.0 ppm. The RTA employs quartz lamps for heating and the temperature is controlled by a calibrated pyrometer. The multilayers were heated at temperatures ranging from 450 to 540 °C for periods of time ranging from 300 to 6.4×10^4 s.

The annealed samples were analyzed by x-ray reflectivity to determine the degree of interdiffusion, described in Sec. I. The measurements were done with a Philips X'Pert system equipped with a Cu anode. Each sample was measured by x-ray reflectivity prior to annealing in the RTA as well as after. In addition, high-resolution transmission electron microscopy cross sections were used to determine the microstructure of the samples. A JEOL JEM 2000-EXII and a Philips TECNAI F20 were used for this.

III. RESULTS

A. X-ray diffraction

Figure 1 shows high angle $\omega-2\theta$ x-ray diffraction spectra for the as-deposited sample, and Table I summarizes information on the spectra. The peak marked (a) at $2\theta = 34.93°$ is the face-centered-cubic (fcc) TaN (111) peak of the cap layer. The cap has a ω-rocking curve with a full width at half maximum (FWHM) of 8.98°. The peak marked (b) at $2\theta = 39.50°$ is the (200) peak of the primitive cubic NiFeCr layer, and this peak has a ω-rocking curve with a FWHM of 7.77°. The third peak in the spectra marked (c) at $2\theta = 43.49°$ is the hexagonal-close-packed (hcp) (0002) peak of the CoFe layers, and the ω-rocking curve has a FWHM of 6.13°, indicating crystalline quality. However, there is a faint hcp Ru (0002) peak overlapping the CoFe peak, as seen by the slight broadening at the low angle side of the (c) peak. Centered around $2\theta = 69.1°$, is the Si (400) peak from the wafer, the Ni *K* absorption edge, a W peak from anode contamination, and the Si (400) peak from Cu $K\beta$ radiation can also be seen. Peak (e) is the higher order (400) peak of the NiFeCr peak. Peaks (f) and (g) are the higher order of double peak (c), peak (f) is the Ru (0004) peak and (g) is the (0004) CoFe peak.

TABLE I. Indicated are the peak index from Fig. 1, the layer that causes the peak, the crystallographic orientation for the layer, the 2θ position of the peak and its full width at half maximum for the rocking curve of the peak.

Index	Layer	Peak	2θ (deg)	FWHM (deg)
a	TaN	(111)	32.93	8.98
b	NiFeCr	(200)	39.50	7.77
c	CoFe	(0002)	43.49	6.13
d	Si	(400)	69.10	···
e	NiFeCr	(400)	85.03	···
f	Ru	(0004)	90.10	···
g	CoFe	(0004)	95.53	···

Figure 2 shows x-ray diffraction pole figures measured in a grid of $2°\times2°$ steps for ϕ (0° – 360°) and ψ (0° – 90°). The pole figures were measured for $2\theta = 34.9°$, 39.5° and 43.4°. In Fig. 2(a) the peak marked (1) is the fcc TaN (111) peak of the capping layer expected at $2\theta = 34.9°$ and psi = 0°. The circle marked (2) at psi = 70.53° is the expected remaining set of visible TaN{111} peaks. It shows that the capping layer has a fiber texture since the peak is present for all the values of phi (0° – 360°) and no threefold symmetry is visible. Figure 2(b), measured at $2\theta = 39.5°$, shows the NiFeCr (200) peak marked (6) in the center and again psi = 90° [the circle is marked (7)]. The fact that peak (7) is present for all phi values (0° – 360°) is indicative of fiber texture that originates in the NiFeCr layer. Figure 2(c), at $\omega-2\theta = 43.4°$, shows the CoFe/Ru (0002) peak in the center, marked (8), and the Si (220) peaks, at psi = 45°, from the substrate. The fact that there is a fiber texture in the seed as well as in the cap makes it plausible that the multilayer is fiber textured as well.

Figure 3 shows typical x-ray reflectivity intensity data for the first multilayer peak at $2\theta = 3.6°$. The data show how the intensity decreases with the length of annealing time. Surrounding the multilayer peaks are also intensity oscillations that come from diffraction of the total stack thickness, as opposed to the thickness that is periodically repeated throughout the structure that gives rise to the multilayer peak itself. It should be pointed out that each intensity measurement is made on a separately annealed sample and that each sample is measured by x-ray reflectivity both prior to annealing, I_0, as well as after, *I*. Thus, any comparison of intensity ratios I/I_0 correctly reflects the decrease in intensity and has no relation to the sample size or other similar factors.

Figure 4(a) shows the normalized intensity I/I_0 for all the different annealing temperatures used in the study (450, 470, 480, 490, 500, 510, 520, and 540 °C). The intensity decreases in linear fashion with $\ln(I/I_0)$ over time as expected from Eq. (2). Normally the relationship in the plot generates a straight line starting from $\ln(I/I_0)=1$, however, the initial phase will relieve some stress in the film and it is usually nonlinear. It can be seen in the enlarged portion in Fig. 4(b) that the lines do not really meet $\ln(I/I_0)=1$. In Fig. 5 the diffusion rates are plotted in an Arrhenius plot. There is a single change in rate with the temperature which is described by an activation energy of $E_a = 4.95$ eV and a prefactor of

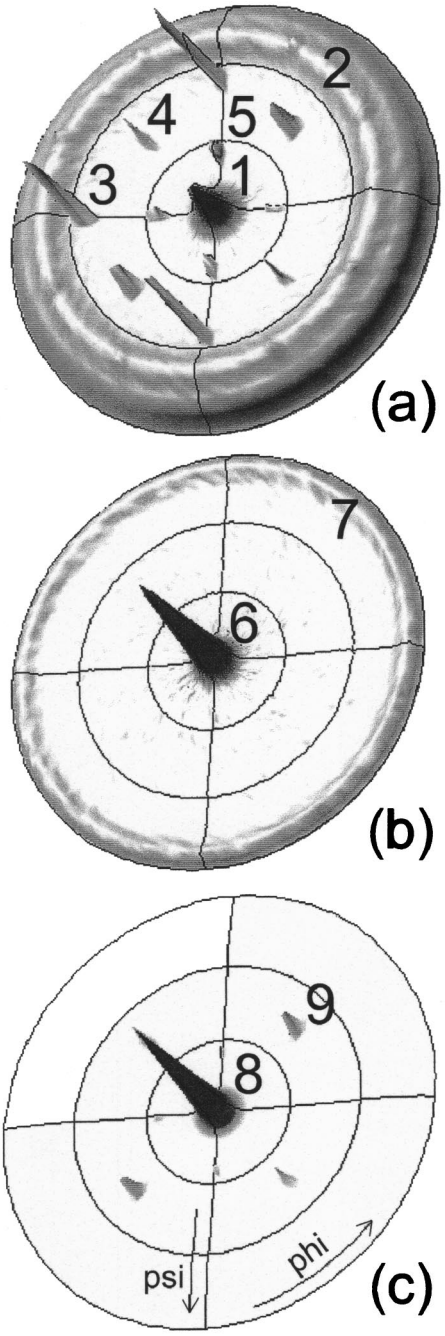

FIG. 2. X-ray diffraction pole figures for $2\theta =$ (a) 34.9°, (b) 39.5° and (c) 43.4°. In (a) the peak marked (1) is the fcc TaN (111) peak. The circle marked (2) at 70.5° is the TaN {111} plane set expected at 70.5°. The additional peaks marked (3), (4), and (5) are the Si (111), (220), and (113) peaks, respectively, from the single crystalline (*l*00) oriented Si substrate. (b) Primitive cubic NiFeCr (200) peak marked (6) in the center and again at psi = 90°, marked (7). (c) CoFe/Ru (0002) peak in the center, marked (8), and the Si (220) peaks, at psi = 45°, from the substrate.

$D_0 = 6.43 \times 10^{-9}\ \mathrm{m}^2/\mathrm{s}$. As is seen, the data are a linear function of ln(D) in the whole temperature interval. The linearity of the whole region implies that there is only one activation energy, that of bulk diffusion or grain boundary diffusion.

Figure 6 shows cross sectional transmission electron microscopy (TEM) images of the multilayered sample structure

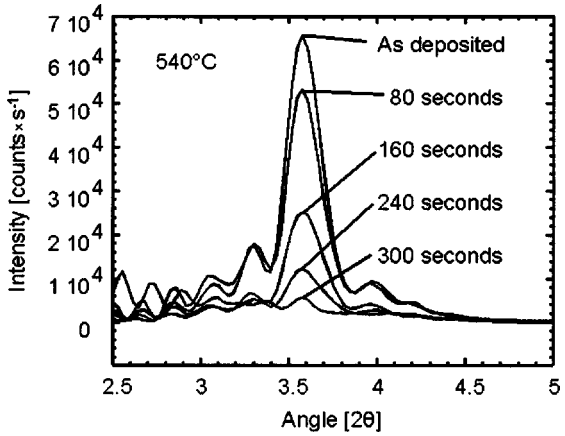

FIG. 3. X-ray reflectivity intensity data for the first multilayer peak at $2\theta = 3.6°$. The intensity, I, is seen to decrease with the annealing time. The temperature of the anneal was 540 °C. Intensity data are shown for 80, 160, 240, and 300 s as well as for the as-deposited intensity.

for the as-deposited film, a film annealed at 500 °C for 20 min and a film annealed at 540 °C for 20 min. In both Fig. 6(a) and 6(b) the CoFe/Ru multilayer structure can be clearly seen together with the TaN cap and the NiFeCr seed layer,

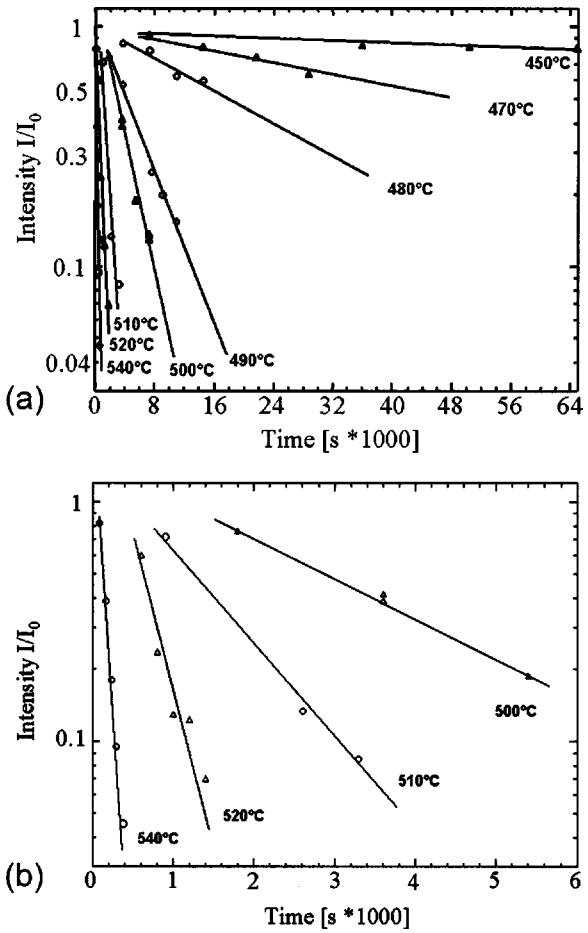

FIG. 4. (a) X-ray diffraction intensity data for different annealing times and temperatures. The intensity, I, is normalized to the intensity prior to annealing, I_0. The temperatures were 450, 470, 480, 490, 500, 510, 520, and 540 °C. The annealing times varied from 300 to 6.4×10^4 s. (b) Enlargement of the time from 0 to 6000 s that show the data for the shorter times/higher temperatures more clearly.

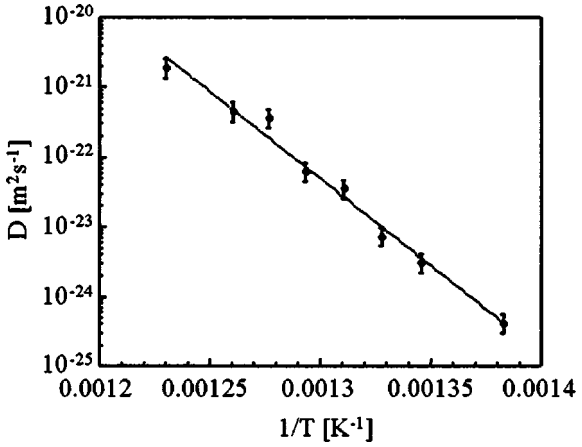

FIG. 5. Diffusion data for the $Co_{90}Fe_{10}$/Ru system in an Arrhenius plot. The diffusion rates are plotted vs $1/T$. There is one diffusion rate which is described by an activation energy of $E_a = 4.95 \pm 0.25$ eV and a prefactor of $D_0 = 6.43 \times 10^{-9}$ m^2/s.

even though diffusion has reduced the intensity ratio I/I_0 in Fig. 6(b) to ~ 0.87. In Fig. 6(c), on the other hand, the CoFe/Ru multilayer structure as well as the seed layer are lost; only the TaN cap is unaffected by annealing. Figure 7 shows $1.0 \times 0.5\ \mu$m^2 atomic force microscopy images of the TaN surface of the, as-deposited film and that annealed at

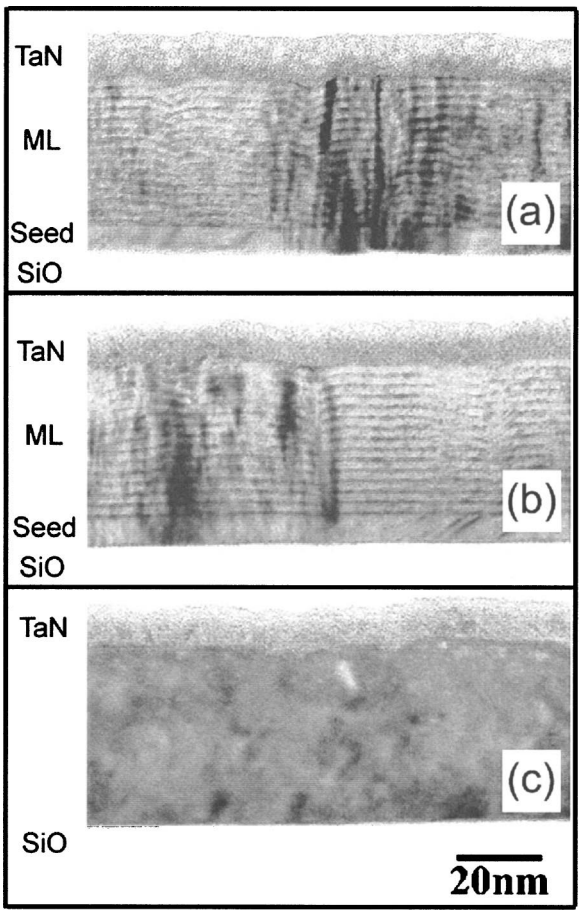

FIG. 6. TEM images of the sample structure for (a) the as-deposited film, (b) a film annealed at 500 °C for 20 min and (c) a film annealed at 540 °C for 20 min.

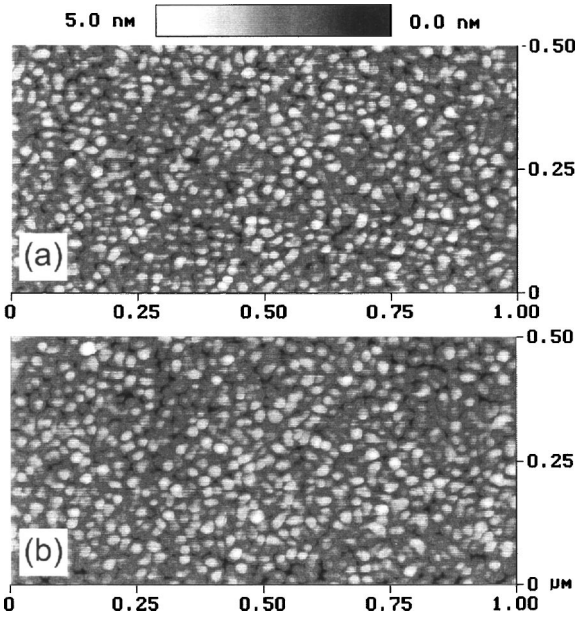

FIG. 7. $1 \times 0.5\ \mu$m^2 atomic force microscopy images of the TaN surface of the (a) as-deposited film and (b) the film annealed until the multilayer structure is completely interdiffused.

540 °C for 20 min; the two images have the same surface feature size and surface roughness. The fact that the images are identical shows that the cap layer is unaffected by the annealing process and as such protects the multilayer during the annealing process without ''participating'' in the reaction.

B. Transmission electron diffraction

Electron diffraction patterns from plan view TEM images are shown in Figs. 8(a)–8(c). The diffraction patterns were taken from areas approximately 500 nm$\times$500 nm in all three images. Figure 8(a) shows an electron diffraction pattern from a single crystallographic domain, while Fig. 8(b) shows an electron diffraction pattern from a slightly different area that displays two patterns rotated 60° to each other. The enlarged electron diffraction pattern area in Fig. 8(c) from the single domain pattern in Fig. 8(a) is indexed and shows the TaN (111), Ru $(10\bar{1}0)$ and the CoFe $(10\bar{1}0)$ spots as well as the Ru $(11\bar{2}0)$ and the CoFe $(11\bar{2}0)$ and higher orders of Ru $(10\bar{1}0)$ and CoFe $(10\bar{1}0)$ spots. The diffraction patterns are consistent with x-ray diffraction data regarding the out of plane orientation of the layers. However, the TEM data are derived from a smaller sample area and as such not show the fiber texture in the plane as the x-ray data, but instead show only one or a few crystallographic domains.

A selected area TEM was produced for an as-deposited sample. In Fig. 9 the diffraction pattern is shown in the inset with an arrow marking the selected double $(10\bar{1}0)$ diffraction spot. The TEM plan view in Fig. 9 shows the size of the grains in the structure. The estimated grain boundary area is 9.0×10^4 nm^2 for each μm^3 of multilayer film. The grains are very large in comparison to what is normally observed for thin films deposited at room temperature and as a consequence the samples have very little grain boundary area.

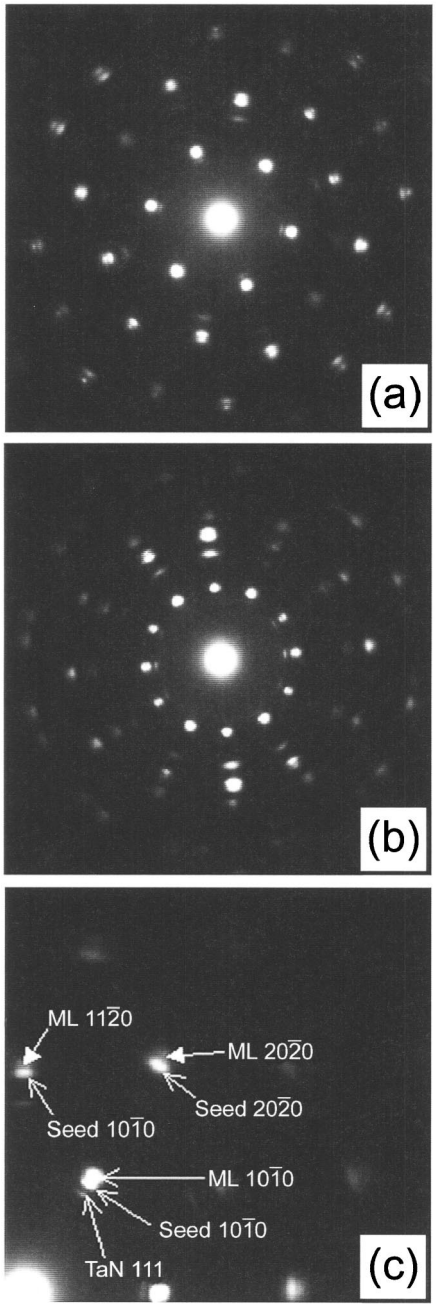

FIG. 8. Electron diffraction patterns from a plan view TEM image of (a) single domain, (b) dual domains rotated 30° to each other that produce a high symmetry boundary between the two domains and (c) enlargement of the single domain pattern with spots indexed to the TaN cap and the Ru/CoFe multilayer constituents.

Figure 10 shows a high resolution TEM image of the as-deposited sample structure close to the substrate. Region (a) indicates the amorphous SiO_2 substrate whereas region (b) is an amorphous initial layer of the NiFeCr seed. Region (c) is a crystalline region of the NiFeCr seed. Region (d) indicates the first few bilayers of the CoFe/Ru multilayer structure. The magnified region shows an area with a cusp in the layer structure, still, the continuous (0002) lattice fringes show that it is a continuous crystal structure throughout the area. The large size of the crystalline domains is probably a result of the fact that the NiFeCr seed is initially amorphous,

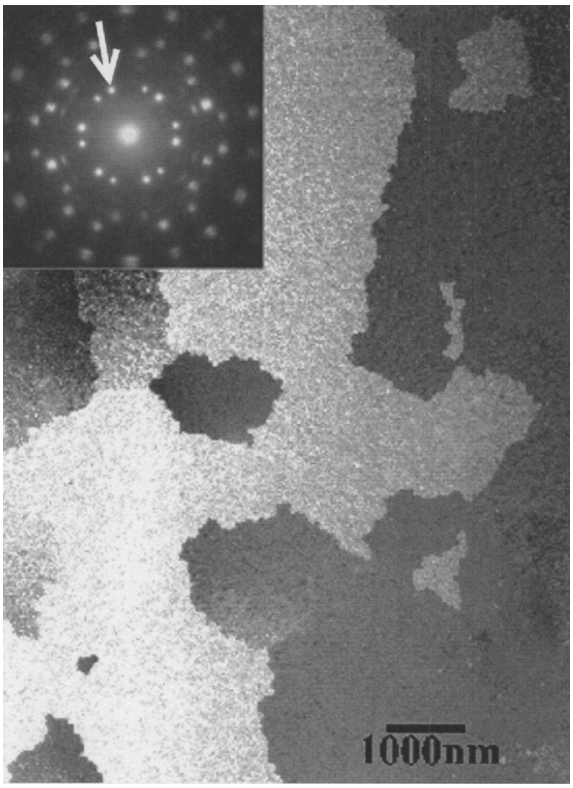

FIG. 9. Selected area TEM image of the as-deposited sample. The inset shows the diffraction pattern, indicating two grain orientations within the image. The white arrow indicates the spot selected for the image. In this case the two domain orientations seen are rotated 15° to each other, producing a high symmetry boundary.

instead of exhibiting an immediate transformation to a crystalline structure. An immediate transformation would most likely take place, or ''nucleate,'' simultaneously with higher density.

In Fig. 11 another part of the multilayer structure is shown within the high resolution TEM image. The $(10\bar{1}1)$ set of lattice fringes is resolved, but some dislocations are present. This can be seen in the inset, which shows slight misalignment in the $(10\bar{1}1)$ planes in consecutive CoFe layers, indicative of different lattice spacing in the CoFe and Ru layers. The misalignment is an indication that even though the layered structure is only one crystal, there is a change in the lattice parameter between the different layers.

IV. DISCUSSION

The high angle $\omega-2\theta$ x-ray diffraction spectra for the as-deposited sample shown in Fig. 1 has a CoFe peak from the multilayer at $2\theta=43.49°$, indicating an approximate average out-of-plane lattice parameter spacing of 0.208 nm. The layer thus has an average lattice parameter that is between that of Ru with $a_{\mathrm{Ru}}=0.270\,58$ nm, $c_{\mathrm{Ru}}=0.428\,19$ nm ($c_{\mathrm{Ru}}/2=0.214$ nm) and Co with $a_{\mathrm{Co}}=0.250\,31$ nm, $c_{\mathrm{Co}}=0.406\,05$ nm ($c_{\mathrm{Co}}/2=0.203$ nm). The smaller constituent Fe has a lattice parameter of $a_{\mathrm{Fe}}=0.2451$ nm and $c_{\mathrm{Fe}}=0.3931$ nm ($c_{\mathrm{Fe}}/2=0.197$ nm). From Vegard's law one would expect a multilayer (ML) out-of-plane lattice parameter of $c_{\mathrm{ML}}=0.206$ nm, however, that

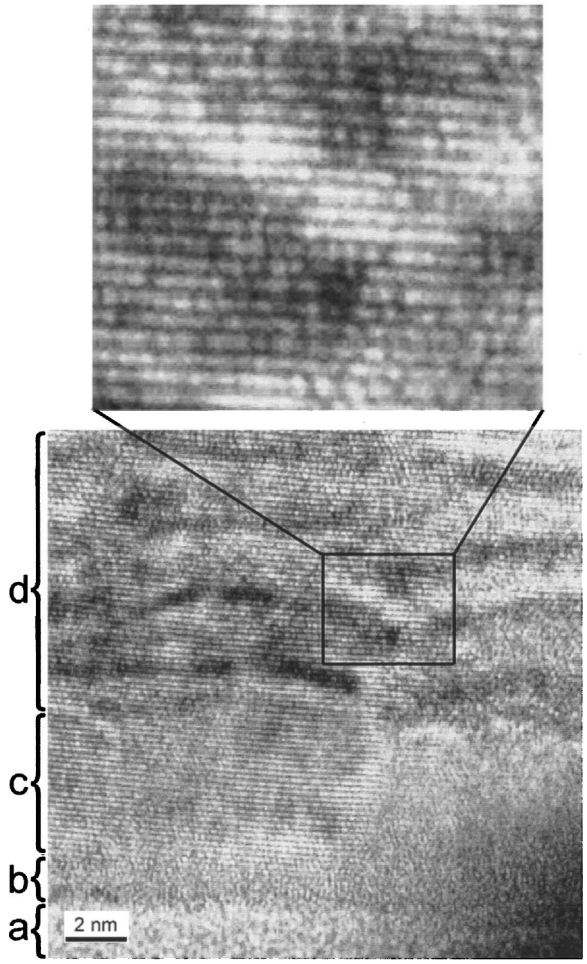

FIG. 10. High resolution TEM image of the sample structure. Region (a) indicates the amorphous SiO substrate whereas region (b) is an initial amorphous region of the NiFeCr seed. Region (c) is a crystalline region of the NiFeCr seed. Region (d) indicates the first few bilayers of the CoFe/Ru multilayer structure. The magnified region shows an area with a cusp in the layer structure and that it is a continuous crystal structure throughout the area.

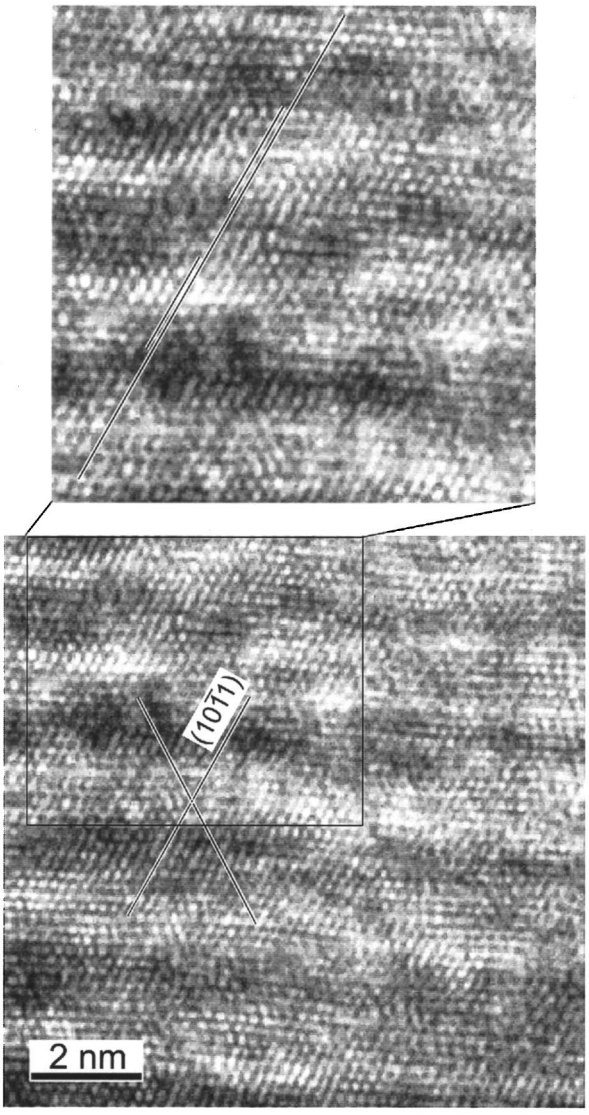

FIG. 11. High resolution TEM image of the multilayer structure. In the image the $(10\bar{1}1)$ set of lattice fringes is resolved. The enlarged region shows slight misalignment of the planes in consecutive CoFe layers.

does not take into consideration the differences in stiffness among Ru, Co and Fe, which makes the value of 0.208 nm plausible. The separation of the higher order peaks for the multilayer constituents indicates that the use of an average multilayer lattice parameter is not completely accurate. By using the Ru and CoFe (0004) peaks that are clearly separated at $2\theta = 90.15°$ and $95.65°$ the lattice (0004) spacing in the Ru layers is given by $d_{\mathrm{Ru}\,(0004)} = 1.0879$ nm and for CoFe by $d_{\mathrm{CoFe}\,(0004)} = 1.0394$ nm. The position of the (0004) peaks indicates a shift (enlargement) of the *c*-axis parameter for Ru to $\Delta c_{\mathrm{Ru}} = 0.0068$ nm and for CoFe to $\Delta c_{\mathrm{CoFe}} = 0.0304$ nm compared to bulk values. Since both increase instead of shifting towards an average value there is probably stress in the film. The accuracy in the determination of the Si (004) peak and hence the diffractometer measurement is $\Delta c_{\mathrm{Si}} = 0.0012$ nm, almost an order of magnitude smaller than the shifts. The fact that the CoFe *c* axis is ~96% of the Ru *c* axis can also be seen as a shift in the $(10\bar{1}1)$ lattice fringes, for consecutive CoFe layers, in the inset of the TEM image in Fig. 11. The TaN (111) peak from the cap layer at $2\theta = 34.93°$ and the (0002) peak of NiFeCr at $2\theta = 39.50°$ are both at the positions expected in the x-ray spectra.

The x-ray diffraction pole figures in Fig. 2 measured at 2θ values of $2\theta = 34.9°$, $39.5°$ and $43.4°$ are representative of fcc TaN (111), primitive cubic NiFeCr (200), and hcp CoFe (0002), respectively. It is possible to conclude that there is a fiber texture in the multilayer from two pieces of data. First, the pole figures in Fig. 2 indicate a fiber texture in the top most TaN layer. Second, the TEM electron diffraction pattern in Fig. 8(c) indicates perfect registry, within a grain, of the crystal orientation of the bottom NiFeCr seed throughout the multilayer up to the TaN cap. Thus, when the overall film shows a fiber texture in the TaN layer the multilayer must have it as well. The intensity seen in Fig. 2(b) seems to peak at psi ~85°, marked (7), and the reason it peaks at ~85° instead of at 90° is a result of the reduced intensity when tilting the sample surface almost parallel to the x-ray beam. From Fig. 10 it can be seen that the crystal-

line (200) structure first develops during deposition of the NiFeCr seed layer (after ~2 nm). The high resolution TEM shows the crystalline structure to be continuos throughout the multilayer. These measurements show that the sample consists of rather large grains within the multilayer that has a hcp structure that is inherited from the NiFeCr seed.

Experimental self-diffusion data for Fe have given activation energies in the range of ~2.5−3.2 eV, depending on several factors, such as crystal structure. Co is reported[8] to have an activation energy of ~3.1 eV, and Hu *et al.* calculated[9] the ruthenium activation energy for vacancy and divacancy diffusion to be ~3.7 eV. The diffusion activation energy for equiatomic CoFe crystals has been determined from the isotope effect by Fishman *et al.* for different crystallographic phases.[10] In their work they determined that the activation energy was lower for the body-centered-cubic (bcc) phase than for the fcc. The activation energies for diffusion were 2.97 and 3.01 eV for Fe and Co, respectively, in the fcc structure, and 2.38 and 2.60 eV for Fe and Co, respectively, in the bcc structure. However, for CoFe in a CsCl structure the activation energy for interdiffusion was determined to be 5.77 eV, and it might be associated with a different diffusion mechanism. In systems with higher melting points than Co, Fe, and Ru, activation energies of over 5 eV has been reported. For example, interdiffusion in the Ta–W system[11] has an activation energy of 5.76 e*V* at 70% W in the temperature range of 1300 – 2100 °C. One of the few reports[12] on diffusion that involve Ru found that the activation energy for bulk diffusion in monocrystalline Cu of $^{103}_{Ru}$ has an activation energy of 2.67 eV. It should be pointed out that the data in our work have not taken into account the stress in the film. Cook and de Fontaine[13] and others[14] have shown that the interdiffusion coefficient is dependent on stress and concentration gradients within a multilayer.

The CoFe/Ru multilayer in this study has a hexagonal-close-packed structure and activation energy of 4.95 eV in the temperature range of 450 – 540 °C. In the temperature interval 450 – 540 °C, the diffusion coefficient changes almost four orders of magnitude from $D=5\times10^{-25}$ to $2\times10^{-21}\,m^2/s$. Given the diffusion constants at 500 and 540 °C ($D_{500}=6.38\times10^{-23}\,m^2/s$ and $D_{540}=1.93\times10^{-21}\,m^2/s$), the linear distance traveled in 20 min in a simple random walk is 0.28 and 1.5 nm, respectively. This is consistent with the TEM cross sections in Fig. 6: For the sample annealed at 500 °C [Fig. 6(b)], the multilayer structure can still be clearly resolved, whereas it is completely lost for the sample annealed at 540 °C [Fig. 6(c)].

It was expected from previous experiments with NiFeCr seed layers and CoFe/Cu multilayers[15] that grain boundary diffusion would be present in the temperature range studied. However, only a single slope is apparent in Fig. 5, and the activation energy is too high to be attributed to grain boundary diffusion. Usually, grain boundary diffusion is observed at temperatures below approximately two thirds of the melting point. For Ru, Co, and Fe the melting points are $T_{Ru}=2607$ K, $T_{Co}=1768$ K and $T_{Fe}=1811$ K. Thus, for Co, one would expect to see grain boundary diffusion below 905 °C.

One explanation for the absence of grain boundary diffusion in our samples could be that there are no grain boundary diffusion paths in these multilayers because of large grains and high symmetry grain boundaries. The x-ray pole figures in Fig. 2 indicate that, on a large length scale (millimeters), there is fiber texture in the samples, thus they contain grains with random orientation in the plane. On a smaller scale (micrometers) it can be seen from the TEM images in Figs. 8 and 9 that the grains are very large and that the neighboring grains have specific high symmetry rotational relationships. The estimated grain boundary area is $9.0\times10^4\,nm^2$ for each μm^3 of multilayer film. This should be compared to $5.2\times10^6\,nm^2$ for each μm^3 in similar CoFe/Cu multilayers.[15] Since the grain boundary area is 58 times bigger in the Cu based multilayers one would expect that the effect would not necessarily be seen here. Further, it is well known that the grain boundary diffusion rate varies with the relative angle of rotation, θ, required to bring two neighboring crystallographic axes into rotational alignment. For low values of θ, and values close to the rotational symmetry, the diffusivity decreases.[16] A classic demonstration of the fact that ''good fit'' in the crystal structure does not permit grain boundary diffusion is found in the lead/tin system,[17] where grain boundaries with a small coincidence site lattice[18] showed low grain boundary diffusion. One dislocation model[19] for certain grain boundaries predicts that there are dislocations regularly spaced along the boundary and that the lattice between the dislocation cores is elastically strained but relatively perfect. However, the diffusion in the core of the dislocations is high and acts as a channel for grain boundary diffusion instead of a thin slab along the whole grain boundary. Given the high symmetry of the grain boundaries in our case, and thus the low density of available diffusion paths in the CoFe/Ru multilayer, it is possible that this effect is what is observed in our case.

V. CONCLUSIONS

Diffusion in (0002) oriented polycrystalline $Co_{90}Fe_{10}$/Ru multilayers was measured and quantified by x-ray reflectivity in the temperature range of 450 – 540 °C. The bulk diffusion in this case is described by an activation energy of $E_a=4.95$ eV and a prefactor of $D_0=6.43\times10^{-9}\,m^2/s$. No grain boundary diffusion was observed in the large grain structure dominated by high symmetry grain boundaries. The crystalline structure first develops during deposition of the NiFeCr seed layer (after ~2 nm) and is transferred to the CoFe/Ru multilayer. TEM images also show that cusp-like features within the multilayer are still single crystalline and not grain boundaries. The estimated grain boundary area is $9.0\times10^4\,nm^2$ for each μm^3 of sputtered film.

ACKNOWLEDGMENT

The authors would like to thank Zheng Gao for deposition of the samples used in this study.

[1] R. J. Borg and G. J. Dienes, An Introduction to Solid State Diffusion (Academic, Boston, 1988).
[2] H. E. Cook and J. E. Hilliard, J. Appl. Phys. **40**, 2191 (1969).
[3] M. P. Rosenblum and D. Turnbull, Appl. Phys. Lett. **37**, 184 (1980).
[4] A. L. Greer and F. Spaepen, in *Synthetic Modulated Structures*, edited by

L. L. Chang and B. C. Geissen (Academic, New York, 1985).
[5] J. DuMond and J. P. Youtz, J. Appl. Phys. **11**, 357 (1940).
[6] A. Guinier, *X-ray Diffraction* (Freeman, San Francisco, 1963).
[7] T. Tsakalakos, Ph.D. thesis, Northwestern University, Evanston, Ill, 1977.
[8] Smithell's Metals Reference Book, 7th ed., edited by E. A. Brandes and G. B. Brook (Linacre House, Oxford, UK, 1992), Chap 13.
[9] W. Hu, B. Zhang, B. Huang, F. Gao, and D. J. Bacon, J. Phys.: Condens. Matter **13**, 1193 (2001).
[10] S. G. Fishman, D. Gupta, and D. S. Lieberman, Phys. Rev. B **2**, 1451 (1970).
[11] A. D. Romig, Jr. and M. J. Cieslak, J. Appl. Phys. **58**, 3425 (1985).
[12] J. Bernardini and J. Cabane, Acta. Metall. 21, 1571 (1973); I. Kaur and W. Gust, *Handbook of Grain and Interphase Boundary Diffusion Data* (Ziegler, Stuttgart, Germany, 1989).
[13] H. E. Cook and D. de Fontaine, Acta Metall. **17**, 915 (1969); H. E. Cook and J. E. Hilliard, J. Appl. Phys. **40**, 2191 (1969); H. E. Cook, D. de Fontaine, and J. E. Hilliard, Acta Metall. **17**, 765 (1969).
[14] A. L. Greer and F. Spaepen, Synthetic Modulated Structures, edited by L. L. Chang and B. C. Giessen (Academic, London, 1985).
[15] E. B. Svedberg, K. J. Howard, M. C. Bønsager, B. B. Pant, A. G. Roy, D. E. Laughlin, J. Appl. Phys. (submitted).
[16] F. Weinberg, *Progress in Metal Physics*, edited by B. Chalmers and R. King (Pergamon, New York, 1959), Vol. 8, p. 105.
[17] K. T. Aust and J. W. Rutter, Trans. AIME **215**, 119 (1959).
[18] V. Randle, The Role of the *Coincidence Site Lattice in Grain Boundary Engineering* (The Institute of Materials, London, 1996).
[19] T. Read, Dislocations in *Crystals* (McGraw–Hill, New York, 1953), Chap. 11.